Nanodisturbances and nanoscale deformation twins in fcc nanowires

S. V. Bobylev and I. A. Ovid'ko[*]

Institute of Problems of Mechanical Engineering, Russian Academy of Sciences, Bolshoj 61, Vasilievskii Ostrov, St. Petersburg 199178, Russia
(Received 24 April 2010; published 23 February 2011)

The nanodisturbance deformation mode is theoretically described as a specific physical mechanism of plastic flow in nanowires with a fcc crystal structure. The mode represents formation and evolution of nanodisturbances—nanoscopic areas of ideal plastic shear with tiny shear vectors—in mechanically loaded nanowires. We calculated the energy and stress characteristics for the formation of both isolated nanodisturbances and their groups (whose evolution results in nucleation of deformation twins) in Au and Cu nanowires having square cross sections. It is shown that the nanodisturbance deformation mode tends to dominate over conventional dislocation generation and glide in Au and Cu nanowires (with flat free surfaces) at high stresses and zero temperature. In these nanowires, the critical stress for the formation of isolated nanodisturbances and that for nucleation of deformation twins is sensitive to the nanowire width. The sensitivity corresponds to the "smaller is stronger" tendency.

I. INTRODUCTION

Plastic deformation processes at the nanoscale level strongly influence mechanical and physical properties of various nanostructured solids; see, e.g., Refs. 1–23. In recent years, particular attention has been paid to defect structure evolution and physical mechanisms of plastic deformation in nanometer- and submicrometer-sized wires (hereinafter called nanowires).[11–23] In particular, it was revealed that mechanically loaded nanowires show unusual deformation behavior that is dependent on their sizes. For instance, as it has been demonstrated in experiments[12,14,15,20,23] with metallic fcc nanowires having diameters of ∼200–500 nm, the values of their strength under compression tests are larger by 10–50 times than those of bulk materials with the same chemical composition. Also, such nanowires show pronounced strain hardening under plastic deformation. The experimental data[12,14,15,20,23] pointing to both superior strength and pronounced strain hardening of nanowires have their logical explanation within the idea[14,15] of dislocation starvation. According to this explanation suggested by Greer and Nix,[14,15] preexistent dislocations move in nanowires and rapidly disappear at nanowire free surfaces during the first deformation stage. As a result of the first deformation stage, a nanowire becomes free from dislocations. Then, the second stage of deformation occurs at very high stresses needed to initiate plastic flow of the defect-free nanowire. Also, as has been shown in recent experiments,[17,22] superior strength (close to the theoretical strength) is typical for dislocation-free metallic nanowires with linear sizes of their cross sections ranging from 75 to 1000 nm. In the context discussed, there is much interest in understanding the physical mechanisms that govern plasticity in defect-free nanowires at the nanoscale level. According to computer models[18,19] of plastic flow in initially defect-free nanowires, dislocations nucleate at nanowire free surfaces. In the case of a nanowire with a square cross section, its corners (edges) serve as preferred sites for dislocation nucleation.[19] In the case of a cylinderlike nanowire, dislocation nucleation preferably occurs at the nanowire free surface in the vicinity of thin strips of atoms on otherwise flat terraces.[18] In addition, the formation of nanoscale deformation twins has

been observed in a computer model[11] of plastic deformation in initially defect-free, single-crystalline Cu nanowires.

Recently, in Ref. 24, a specific mechanism of plastic deformation in defect-free nanowires has been suggested. This mechanism represents formation of near-surface nanodisturbances—nanoscopic areas of plastic shear with tiny shear vectors—in single-crystalline nanowires under mechanical load. Deformation-induced formation of isolated stacking faults without the involvement of any dislocations in nanowires with extra small sizes was predicted.[24] This prediction has been indirectly confirmed by the experimental observation[25] of isolated stacking faults in Au nanowires with lateral sizes ∼5 nm or smaller. In Ref. 24 the nanodisturbance deformation mode was briefly described within a two-dimensional simple model. In particular, we used the simplification that the nanodisturbance deformation mode and conventional lattice dislocation slip in a nanowire with a square cross section do not depend on the coordinate along one edge of the square cross section.[24] The main aim of this paper is to elaborate a three-dimensional theoretical description of the nanodisturbance deformation mode as a specific mechanism of plastic deformation mechanism in defect-free nanowires with a fcc crystal lattice, taking into account the role of nanowire corners (edges) as the preferred nucleation sites for plastic shear. Also, we will theoretically describe the role of nanodisturbances (consequently formed at neighboring crystallographic planes) as nuclei of nanoscale deformation twins in fcc nanowires.

II. GEOMETRY OF NANODISTURBANCE DEFORMATION MODE IN fcc NANOWIRES

Let us consider plastic deformation of a single-crystalline fcc metal nanowire having an initial shape of a long rectangular box [Fig. 1(a)]. A square section of the nanowire has a size $d \times d$ [Fig. 1(a)]. In the situation where the nanowire is free from defects, its plastic flow can occur through conventional nucleation of dislocations at a nanowire free surface and their further glide across a nanowire cross section [Figs. 1(a)–1(e)].[18,19] In addition, following Ref. 24, plastic flow in the nanowire can occur in an alternative way through the formation
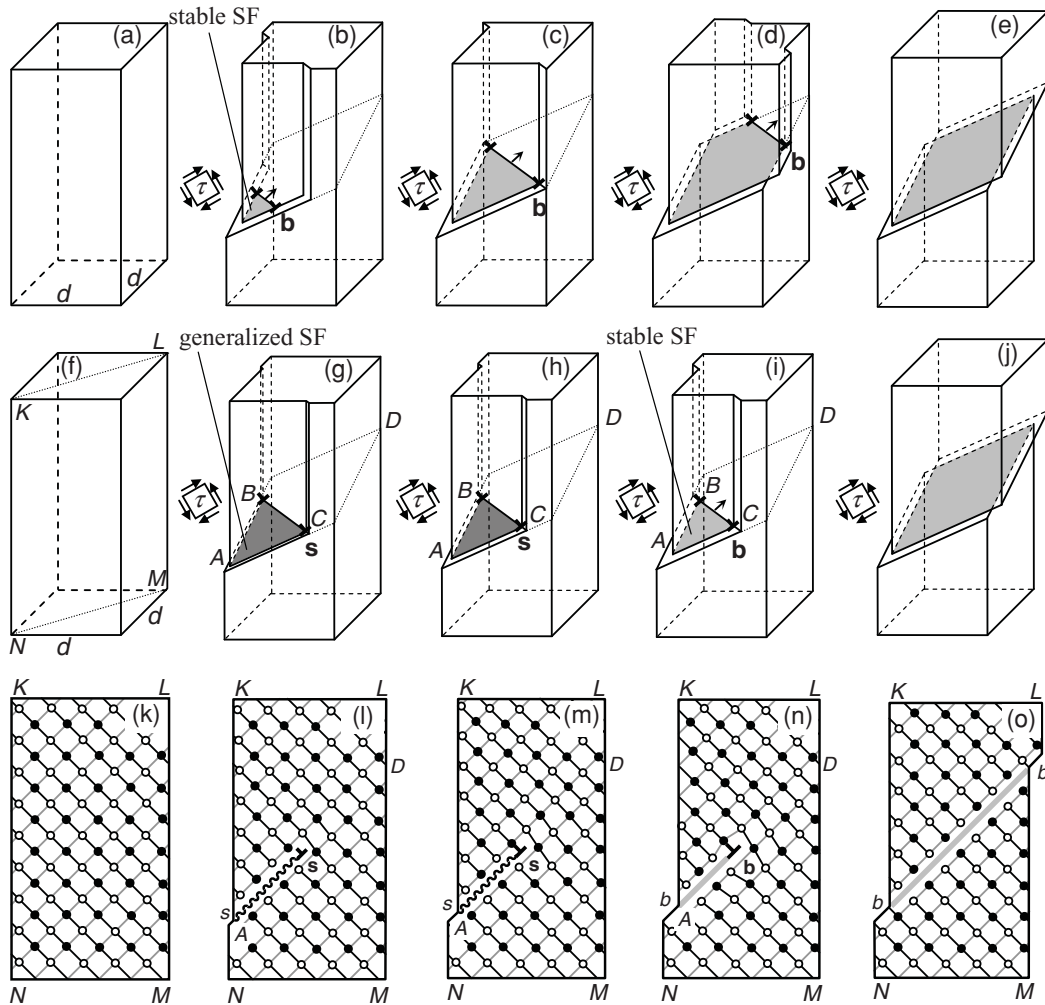
FIG. 1. Plastic deformation modes in nanowires. (a)–(e) Conventional partial dislocation slip. (a) Initial state. (b)–(e) Conventional partial dislocation with Burgers vector **b** is generated at the nanowire free surfaces (where steps of width b are formed) and slips towards opposite free surfaces. A stable stacking fault (SF) joins the dislocation and the free surfaces at which the dislocation was generated. (f)–(j) Nanodisturbance deformation mode (three-dimensional view). (f) Initial state. (g) and (h) Immobile noncrystallographic dislocation is generated. Its Burgers vector magnitude s gradually increases, and a generalized stacking fault (gray region) is formed (and evolves in parallel with the growth of s) between the dislocation and free-surface steps. (i) The partial dislocation transforms into a conventional partial dislocation (when s reaches the magnitude b of the Burgers vector of a conventional partial dislocation) and then moves toward the opposite free surfaces. (j) The final structure with surface steps of width b is formed. (k)–(o) Two-dimensional view of the nanodisturbance deformation mode in a crystallographic plane (containing slip line AD) of a nanowire with a cubic elementary cell containing atoms of two sorts (full and open circles).

of near-surface nanodisturbances, nanoscopic areas of plastic shear with tiny shear vectors [Figs. 1(f)–1(j)].

Let us discuss the geometric details of the alternative deformation mechanism. They are illustrated in both a general three-dimensional view of a nanowire under tensile deformation in Figs. 1(f)–1(j) and a two-dimensional view of a crystallographic plane serving as a model of the diagonal cross section $KLMN$ [Fig. 1(f)] of the nanowire in Figs. 1(k)–1(o). With the real crystallography of fcc nanowires taken into account, it is logical to expect that a nanodisturbance is formed in the rhombic slip plane {111}. At the initial stage, an applied shear stress initiates a "momentary" ideal (rigid-body) shear occurring along the nanoscale fragment ABC of the slip plane. Such a shear is characterized by a tiny shear magnitude s and produces a generalized stacking fault ABC having nanoscale sizes [Figs. 1(g) and 1(l)]. [In the

theory of crystals, a generalized stacking fault is defined as a planar defect resulted from a cut of a perfect crystal across a single plane into two parts, which are then subjected to a relative displacement through an arbitrary vector **s** (lying in the cut plane) and rejoined; see e.g., Refs. 26 and 27.] In the nanowire interior, the generalized stacking fault is bounded by a "noncrystallographic" partial dislocation BC characterized by a nonquantized (noncrystallographic) Burgers vector **s** with a very small magnitude $s < b$, where b is the magnitude of the Burgers vector of a conventional "crystallographic" partial dislocation [Figs. 1(g) and 1(l)]. This defect configuration is called the near-surface nanodisturbance.[24] At the following stage, the magnitude s continuously increases [Figs. 1(h) and 1(m)]. In parallel with the increase in s, the noncrystallographic partial can move. Then, magnitude s reaches magnitude b, and the nanodisturbance transforms into a conventional partial
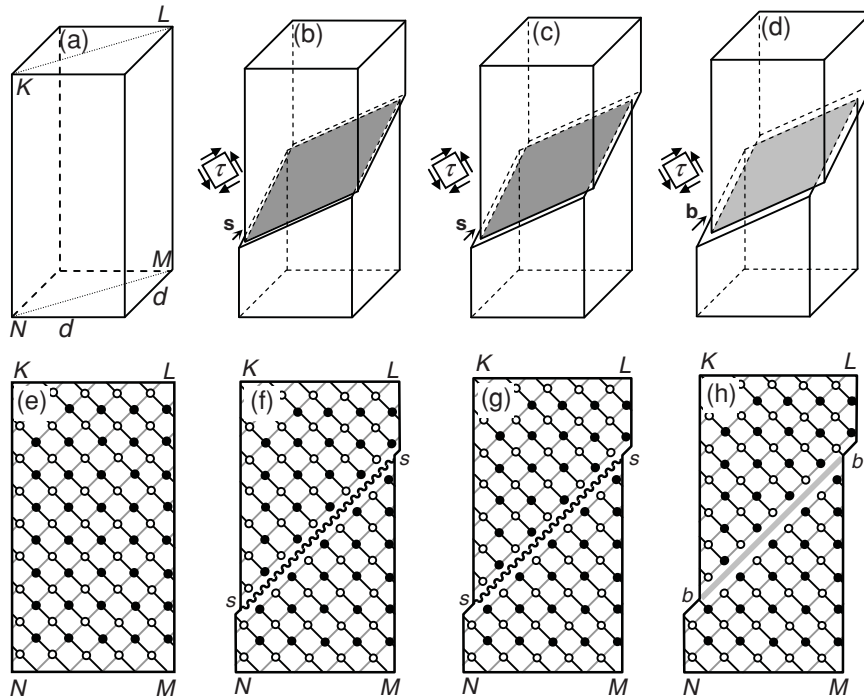
FIG. 2. Nanodisturbance deformation mode in the limiting situation where a nanodisturbance occupies a whole area of a nanowire section. In this situation, the nanodisturbance consists of only a generalized stacking fault and produces steps at the nanowire free surface, while noncrystallographic dislocations are absent.

dislocation joint by a stable stacking fault (a generalized stacking fault with minimum energy) ABC with the free surface [Figs. 1(i) and 1(n)]. The conventional partial dislocation moves and disappears at the free surface, in which case a stable stacking fault is formed in its path [Figs. 1(j) and 1(o)].

Isolated stable stacking faults (and no dislocations) were experimentally observed in Au nanowires with lateral sizes of ∼5 nm or smaller.[25] This experiment indirectly supports the suggested representations of nanodisturbances as potential carriers of plastic deformation in metallic nanowires. Also, the near-surface nanodisturbances in nanowires [Figs. 1(g)–1(i) and 1(l)–1(n)] are similar to "bulk" nanodisturbances experimentally observed[28] in grain interiors of polycrystals of special titanium alloys called Gum metals. Such "bulk" nanodisturbances were *in situ* observed (by high-resolution electron microscopy) during plastic deformation of Gum metals.[28] The bulk nanodisturbances are bounded by loops of noncrystallographic partial dislocations and nucleate owing to *high shear stresses and a dramatic decrease in some elastic constants*.[28–31] As it has been shown in Ref. 24, the formation of near-surface nanodisturbances occurs as a new deformation mode in nanowires [Figs. 1(g)–1(i) and 1(l)–1(n)] owing to the *nanoscale and free-surface effects*. More precisely, as a consequence of these effects, the stresses created by nanodisturbances are effectively screened in nanowires, in which case the formation of nanodisturbances is enhanced.

Also, recently, nanoscale deformation processes in nanometer-sized single crystals with an approximately spherical shape have been experimentally examined by Sun *et al.*[32] They reported that plastic deformation of nanometer-sized Au and Pt crystals in a wide temperature range is controlled by fast events of plastic shear. These fast events result in the formation of stable stacking faults observed in the experiment.[32] In general, such faults can be formed owing to either the slip of short-lived partial dislocations or the nanodisturbance deformation mode. At the same time,

dislocations were not experimentally observed in nanometer-sized single crystals under plastic deformation.[32] In order to identify the deformation mechanism, Sun *et al.*[32] carried out the corresponding molecular-dynamics simulations. According to the simulations,[32] plastic shear in nanometer-sized single Pt crystals occurs as either the slip of short-lived partial dislocations or a homogeneous instant slip, depending on temperature and applied stress.[32] The latter mechanism, in fact, represents the nanodisturbance deformation mode in the limiting situation where a nanodisturbance occupies a whole area of a nanowire section (Fig. 2). That is, the nanodisturbance consists of only a generalized stacking fault and produces steps at the nanowire free surface, while noncrystallographic dislocations are absent (Fig. 2).

The discussed experiments and computer simulations allow us to conclude that our theoretical representations on nanodisturbances in nanowires [Figs. 1(f)–1(o) and 2] are indirectly supported by (i) the experiment[25] concerning plastic deformation (thinning) of Au nanowires, (ii) the experiment[28] with plastic deformation of Gum metals, and (iii) results[32] of molecular-dynamics simulations of plastic flow in nanometer-sized single crystals having an approximately spherical shape.

III. ENERGY AND STRESS CHARACTERISTICS OF NANODISTURBANCE DEFORMATION MODE IN fcc NANOWIRES

Let us calculate the energy characteristics of the specific and conventional modes of plastic flow in nanowires in the exemplary case shown in Fig. 1. Within our model, we consider a nanowire subjected to a constant tensile load. The formation of a nanodisturbance and evolution (in time) of its characteristics, s and x, represent the plastic response of the nanowire material to this mechanical creeplike test. Plastic shear occurs along a rhombic slip plane {111} making an angle $\arccos(1/\sqrt{3})$ with the square base section (Fig. 1) of the

nanowire. The shear occurs under the shear stress τ acting in the plane $\{111\}$. The nanowire is supposed to be an elastically isotropic solid having a shear modulus G and a Poisson ratio ν.

The specific deformation mode [Figs. 1(g)–1(i) and 1(l)–1(n)] is characterized by the change ΔW_n in the nanowire energy owing to the nanodisturbance formation. The energy change ΔW_n (the difference between the energy of the nanowire with the nanodisturbance and that of the defect-free nanowire) consists of the four terms,

$$\Delta W_n = W_d + W_s + W_{\text{gsf}} - A, \qquad (1)$$

where W_d is the proper energy of the dislocation (per its unit length), W_s is the free-surface energy related to formation of free-surface steps owing to plastic shear across a nanowire section, W_{gsf} is the generalized stacking fault energy, and A is the work spent to the plastic shear.

Let us calculate the proper energy W_d of the dislocation located within a nanowire (Fig. 1). The dislocation line BC is oriented along the [110] direction. In other words, the dislocation line is perpendicular to rectangular section $KLMN$ [Fig. 1(f)] of the nanowire. For illustration, Fig. 3(a) shows a nanowire section that is parallel with the nanowire base and contains the dislocation line. We assume that the nanowire height is much larger than the linear size d of a square section of the nanowire. With this assumption, the nanowire can be approximately considered as a rectangular box of infinite height. In this case, the spatial location of the dislocation is unambiguously described by the distance x between the dislocation line and an edge of the nanowire [Fig. 3(a)]. The length of the line BC is equal to $2x$.

The analytical expression for the proper energy W_d of a dislocation whose line core is not parallel to a free surface in a nanowire with square cross section is unknown. At the same time, it is well known[33] that the free surfaces of solids effectively screen the elastic fields of dislocations. In this circumstance, in the calculation of the proper energy W_d, it is effective to exploit the standard approximation[4,34,35] used in the calculation of the energy of dislocations in nanostructures. In doing so, we divide the dislocation line into segments of infinitesimal length dl. Then we suppose that the proper energy density of each dislocation segment depends only on the distance between the segment and the nearest free surface. More precisely, we approximately take the energy of the
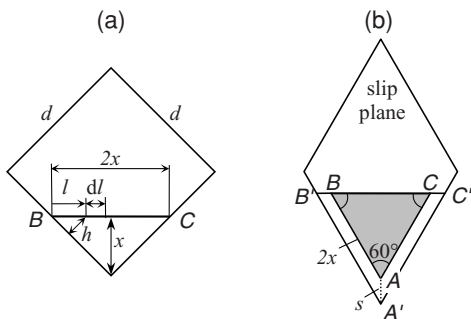

FIG. 3. Geometry of edge dislocation in nanowire (shown schematically). (a) The square nanowire section is parallel with the nanowire base and contains the dislocation line BC. (b) Slip plane of the dislocation BC.

dislocation segment as $dW = (Ds^2/2)\ln(h/s)dl$, where $D = G/[2\pi(1-\nu)]$, s is the dislocation Burgers vector magnitude, where s also serves as the dislocation core radius,[33] and h is the distance between the dislocation segment and the nearest free surface. In the context discussed, h plays the role of screening length for the dislocation stress fields, in the spirit of the textbook formula[33] for the proper elastic energy that equals $(Ds^2/2)\ln(R/r_0)$ of an edge dislocation with the Burgers vector magnitude s, the dislocation core radius r_0, and the screening length R of the dislocation stress fields.

Because the dislocation is not parallel with a free surface, the distance h between a dislocation segment and the nearest free surface is sensitive to the segment position. More precisely, the distance h is given as follows:

$$h(l) = \begin{cases} l/\sqrt{2}, & \text{if } l \leqslant x, \\ (2x-l)/\sqrt{2}, & \text{if } l > x, \end{cases} \qquad (2)$$

where l denotes the distance between a dislocation segment and point B [see Fig. 3(a)]. With formula (2), after integration of the elastic energy $dW = (Ds^2/2)\ln(h/s)dl$ of a dislocation segment along the dislocation line, we find the proper energy of the dislocation under consideration:

$$\begin{aligned} W_d &= W_c + \frac{Ds^2}{2} \int_{s\sqrt{2}}^{2x-s\sqrt{2}} \ln\frac{h(l)}{s}dl \\ &= Ds^2\left(x\ln\frac{x}{s\sqrt{2}} + s\sqrt{2}\right). \end{aligned} \qquad (3)$$

Here the energy W_c of the dislocation core is given as $W_c = Ds^2x$.[33] The value of $s\sqrt{2}$ in the integration limits in formula (3) serves as a cut parameter. When the distance l between a dislocation segment and point B lies within either interval $l < s\sqrt{2}$ or interval $2x - s\sqrt{2} < l < 2x$, the distance between this segment and the free surface is lower than the dislocation core radius s. Therefore, for the discussed intervals of l, we do not take into account contributions of the corresponding dislocation segments into the elastic energy of the dislocation.

Formula (3) is valid within the interval $s\sqrt{2} \leqslant x < d/\sqrt{2}$. In the case of $x > d/\sqrt{2}$, the energy depends in the same way on the distance between the dislocation line and the opposite edge of the nanowire. This allows us to rewrite formula (3) in its general form [valid within the interval $s\sqrt{2} \leqslant x \leqslant (d-s)\sqrt{2}$] as follows:

$$W_d = Ds^2\left[\min(x, d\sqrt{2}-x)\ln\frac{\min(x, d\sqrt{2}-x)}{s\sqrt{2}} + s\sqrt{2}\right]. \qquad (4)$$

The energy W_{gsf} of the stacking fault and work A are given as

$$W_{\text{gsf}} = \gamma_{\text{gsf}}(s)S, \quad A = \tau sS, \qquad (5)$$

respectively. Here $\gamma_{\text{gsf}}(s)$ is the specific energy of the generalized stacking fault (γ_{gsf} is a function of s), and S is the area of a fragment ABC of the slip plane (rhomb) [see Figs. 1 and 3(b)]. With geometry of the fragment ABC [Fig. 3(b)], its area is written as follows:

$$S = \begin{cases} x^2\sqrt{3}, & \text{if } x \leqslant d/\sqrt{2}, \\ [d^2 - (d\sqrt{2}-x)^2]\sqrt{3}, & \text{if } x > d/\sqrt{2}. \end{cases} \qquad (6)$$

The energy W_s of steps at the nanowire free surfaces is evidently given as

$$W_s = \gamma_s S_{\text{step}}, \qquad (7)$$

where γ_s is the specific energy of the free surface (per its unit area), and S_{step} is the sum area of steps at the nanowire free surfaces. Figure 3(b) schematically shows a cross section of the nanowire by the slip plane, in which case the steps have the form of trapezoids ($ABB'A'$ and $ACC'A'$). Their sum area can be approximately written as

$$S_{\text{steps}} \approx 2xs. \qquad (8)$$

Formulas (1), (2), and (4)–(8) allow one to calculate the energy change $\Delta W_n(x,s)$ as a function of variables x and s ranging

within the intervals $b\sqrt{2} < x < (d-b)\sqrt{2}$ and $0 < s \leqslant b$, respectively.

The energy change $\Delta W_n(x,s)$ characterizes the generation and evolution of a nanodisturbance. When $s = b$, formula (1) transforms into the expression for the energy change, specifying classical generation and glide of a lattice partial dislocation. In this context, analysis of the expression (1) allows one to calculate the energy characteristics of both the specific and classical deformation modes as well as to reveal the optimum way of the system evolution. Below, we performed such an analysis in the example case of a Au nanowire with the following typical values of parameters: $G = 27$ GPa, $\nu = 0.44$, and $\gamma_s = 1.48$ J/m^2.[33] The gliding partial dislocation is chosen as an edge Shockley dislocation with Burgers vector magnitude $b = 0.166$ nm. For the generalized
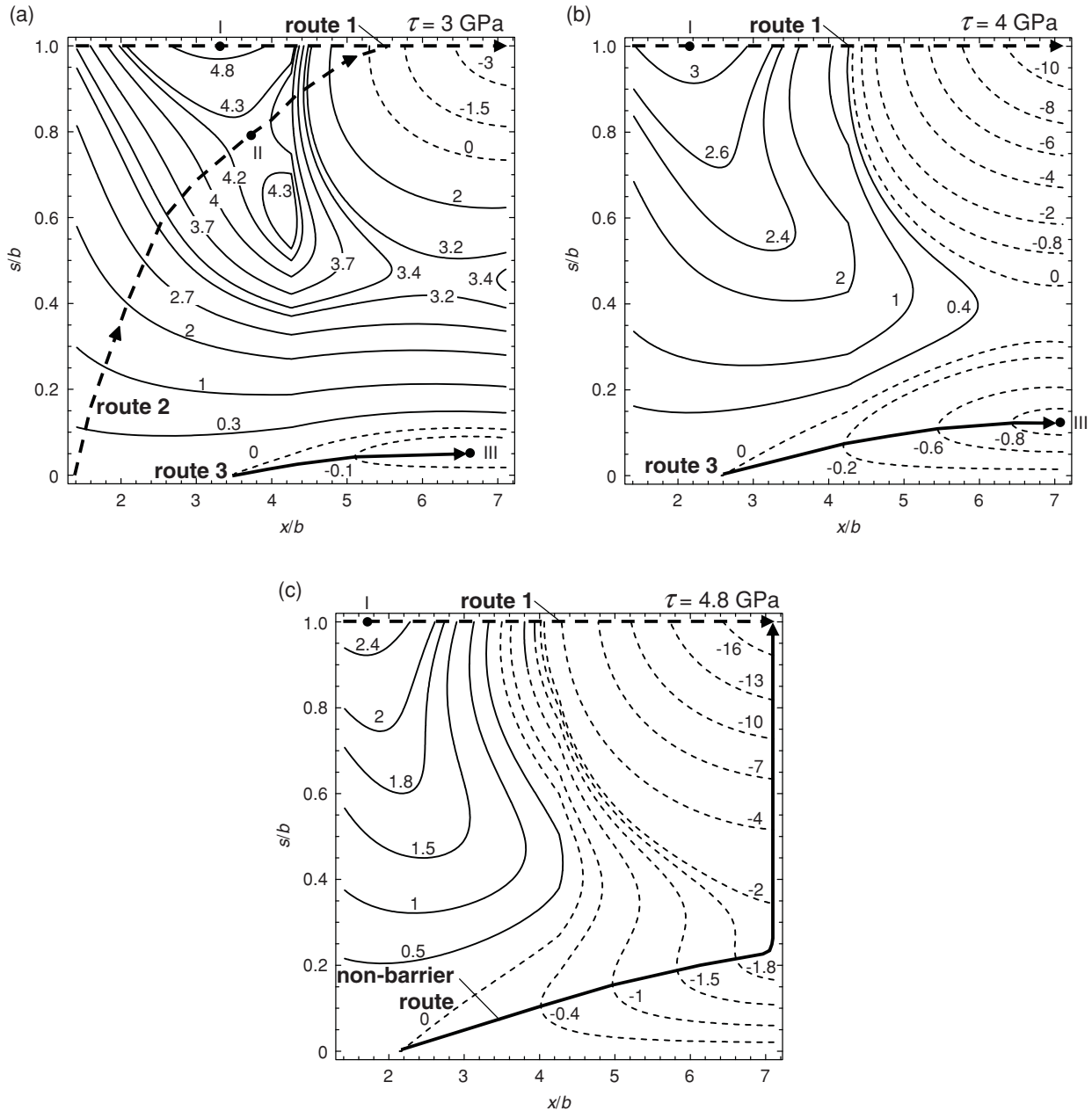

FIG. 4. Maps of the energy change $\Delta W_n(x,s)$ in the case of a Au nanowire (with size $d = 1$ nm) under the external shear stress (a) $\tau = 3$ GPa, (b) $\tau = 4$ GPa, and (c) $\tau = 4.8$ GPa. The values of ΔW_n are given in units of Db^3.
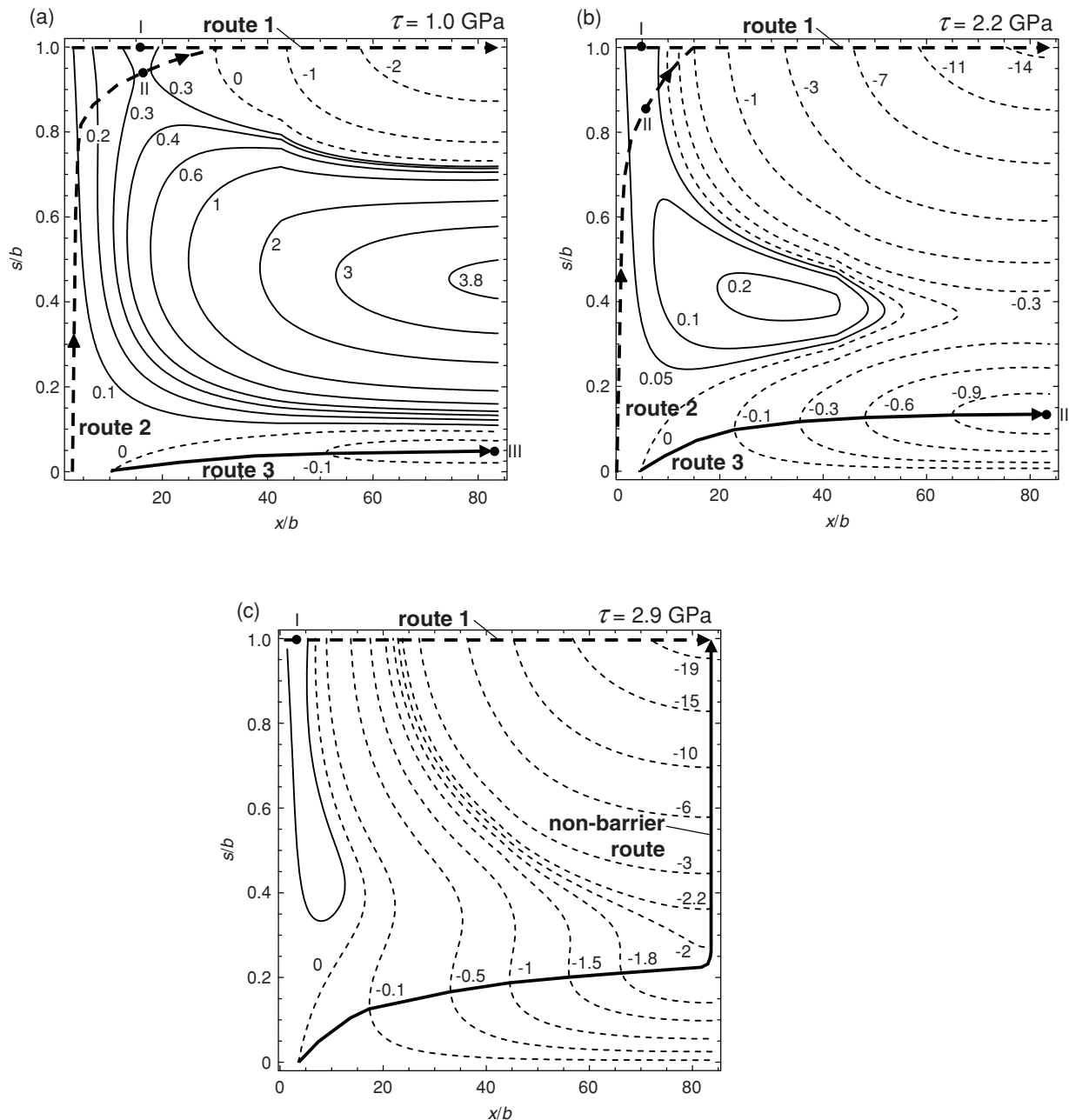
FIG. 5. Maps of the energy change $\Delta W_n(x,s)$ in the case of a Au nanowire (with size $d = 10$ nm) under the external shear stress (a) $\tau = 1$ GPa, (b) $\tau = 2.2$ GPa, and (c) $\tau = 2.9$ GPa. The values of ΔW_n are given in units of 10^2 Db^3.

stacking fault in Au, the dependence $\gamma_{\mathrm{gsf}}(s)$ of its specific energy on s was simulated in Ref. 36. With results from Ref. 36, this dependence can be approximated by the following formula:

$$\gamma_{\mathrm{gsf}}(s/b) = \begin{cases} \frac{\gamma_{\mathrm{us}}}{2}\left(1 - \cos\frac{2\pi s}{b}\right), & 0 \leqslant s/b < 1/2, \\ \frac{\gamma_{\mathrm{us}}+\gamma_{\mathrm{isf}}}{2} - \frac{\gamma_{\mathrm{us}}-\gamma_{\mathrm{isf}}}{2}\cos\frac{2\pi s}{b}, & 1/2 \leqslant s/b < 1. \end{cases} \quad (9)$$

Here γ_{us} and γ_{isf} are the maximum and minimum values of $\gamma_{\mathrm{gsf}}(s)$, respectively. Note that γ_{us} and γ_{isf} characterize unstable and stable configurations of the generalized stacking fault, respectively. In the case of Au, according to simulations presented in Ref. 36, one has $\gamma_{\mathrm{us}} \approx 0.134$ J/m^2 and

$\gamma_{\mathrm{isf}} \approx 0.033$ J/m^2. Using these characteristic values of parameters and formulas (1), (2), and (4)–(9), we calculated the energy maps $\Delta W_n(x,s)$ at different values of external stress in the case of a Au nanowire having the sizes $d = 1$ nm (Fig. 4) and $d = 10$ nm (Fig. 5). The maps allow us to analyze the system evolution in the parameter space (x,s) for both the specific and classical deformation modes.

Within our model, the final defect configuration in a deformed nanowire is specified by the parameter pair [$x = (d-b)\sqrt{2}$, $s = b$] and corresponds to the upper right-hand corner of the energy maps shown in Figs. 4 and 5. In this case, the classical deformation mode corresponds to the arrowed route 1 at the upper part of the map. According to results of

our calculations, there is an energy barrier for the classical deformation mode to occur. The barrier height is indicated at point I of route 1 (Figs. 4 and 5).

In addition, in the energy maps (Figs. 4 and 5), one can distinguish route 2 corresponding to the nanodisturbance deformation mode. Route 2 is specified by the presence of a saddle point II, where the energy value is lower than that at point I. Thus, the nanodisturbance deformation mode (route 2) is characterized by a lower-energy barrier, compared to the classical deformation (route 1). The determination of the saddle-point energies (Figs. 4 and 5) suggests that the results of our model may be applied in the future to related, thermally activated overcoming mechanisms that control the mechanical properties of nanowires.

For definiteness, we consider a zero-temperature situation. For comparatively low values of the stress τ [Figs. 4(a), 4(b), 5(a), and 5(b)], the system at zero temperature evolves through route 3 to a state with the lowest energy (point III), and no barrier exists at the route. However, this state is not the final configuration with $x = (d - b)\sqrt{2}$ and $s = b$. For a low stress level [Figs. 4(a), 4(b), 5(a), and 5(b)], the system at zero temperature never actually reaches the final configuration. For large values of the stress τ, the nanodisturbance mode occurs in the nonbarrier way, and the system reaches the final configuration at zero temperature, in contrast to the classical deformation [see Figs. 4(c) and 5(c)]. In this case, ideal Au nanowires with sizes $d = 1$ and 10 nm are unstable relative to the nanodisturbance deformation. Also, according to our calculations (not presented here), the energy maps $\Delta W_n(x,s)$ are very similar for nanowires having size d in the range from 1 to 300 nm. These results allow us to conclude that the nanodisturbance deformation plays the dominant role in ideal fcc metal nanowires with widely ranged sizes at high stresses and zero temperature.

IV. EFFECTS OF FREE-SURFACE STEPS ON LATTICE DISLOCATION GENERATION AND NANODISTURBANCE DEFORMATION MODE IN fcc NANOWIRES

In real metal nanowires, there are extra factors that influence the competition between the classical dislocation glide [Figs. 1(a)–1(e)] and the nanodisturbance deformation mode [Figs. 1(g)–1(i) and 1(l)–1(n)]. In particular, steps at nanowire free surfaces strongly affect both the processes of the lattice dislocation generation and those of the nanodisturbance formation. For instance, let us consider a fcc metal nanowire having steps at its free surfaces [Fig. 6(a)]. The height of each step is equal to the Burgers vector magnitude b of a partial lattice dislocation. The geometry of the steps enhances the generation of lattice dislocations and nanodisturbances at them, compared to the case of an ideal free surface. It is because the generation processes [Fig. 6(b)] decrease the heights of the free-surface steps. However, the discussed effect for dislocations is different from that for nanodisturbances. When a partial lattice dislocation is generated at a step, the step completely disappears [Fig. 6(b)]. As a result, the energy of the system is decreased by the energy of the free-surface step with height b, and the dislocation generation is greatly enhanced. When a nanodisturbance with a tiny shear
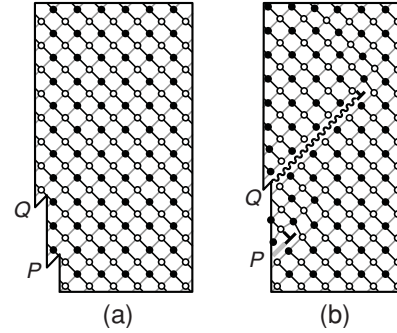

FIG. 6. Generation of a crystallographic partial dislocation and a noncrystallographic dislocation (through the nanodisturbance mechanism) in a nanowire with preexisting steps on the free surface. (a) Initial configuration with steps P and Q. (b) Crystallographic partial dislocation is generated at step P, and nanodisturbance is generated at step Q. As a result, step P disappears (with the assumption that its initial width is equal to the dislocation Burgers vector magnitude), and the step Q width is decreased by the shear magnitude s characterizing the nanodisturbance.

magnitude s is generated at a step, its height is decreased by s ($\ll b$) [Fig. 6(b)]. As a corollary, the energy of the system is decreased by the energy of the free-surface step with height s, and the nanodisturbance generation [Fig. 6(b)] is slightly enhanced. In these circumstances, the classical generation of lattice dislocations at free-surface steps can dominate over the nanodisturbance generation at such steps [Fig. 6(b)].

In order to describe the competition between the classical dislocation glide and the nanodisturbance deformation mode, let us examine the energy change ΔW_n^* that characterizes both processes in question (Fig. 6). In the situation where a nanodisturbance with a tiny shear magnitude s is generated at a free-surface step Q, the energy change ΔW_n^* is described by formula (1) with the term W_s being replaced by $-W_s$. Here W_s is the energy of the free-surface step (created during formation of a nanodisturbance at an ideal free surface and disappearing during the formation of a nanodisturbance at a free-surface step) with height s. That is, we find

$$\Delta W_n^* = W_d - W_s + W_{\text{gsf}} - A, \tag{10}$$

where the terms W_d, W_s, W_{gsf}, and A are described in Sec. III. When $s = b$, formula (10) transforms into the expression for the energy change specifying classical generation and glide of a lattice partial dislocation. In this context, an analysis of expression (10) allows one to calculate and analyze the energy characteristics of both the specific and classical deformation modes.

Figure 7 presents the energy map $\Delta W_n^*(x,s)$ calculated by formula (10) in the case of a Au nanowire (with the size $d = 10$ nm) at an external stress of $\tau = 1.2$ GPa. In contrast to the energy maps corresponding to ideal nanowires (Figs. 4 and 5), the energy map $\Delta W_n^*(x,s)$ shown in Fig. 7 has the nonbarrier route 1 (corresponding to the classical generation and glide of a lattice dislocation). At the same time, the energy barrier exists for the evolution through route 3 (corresponding to the nanodisturbance deformation mode) toward the final configuration [$x = (d - b)\sqrt{2}$, $s = b$]. Thus,
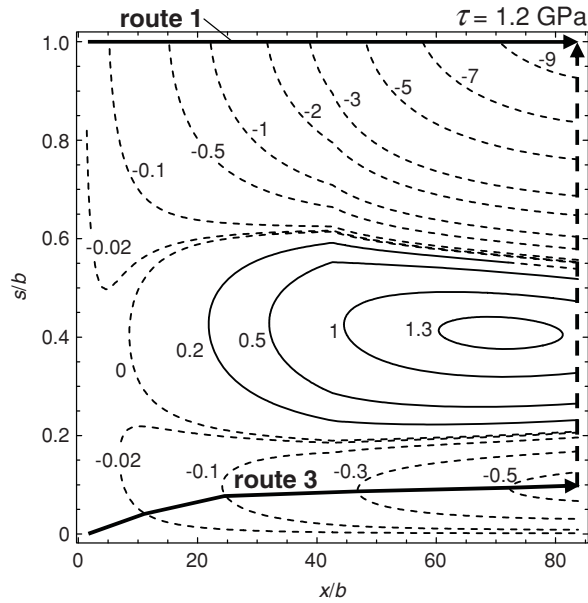
FIG. 7. Map of the energy change $\Delta W_n^*(x,s)$ in the case of a Au nanowire with size $d = 10$ nm under the external shear stress $\tau = 1.2$ GPa. The values of ΔW_n^* are given in units of 10^2 Db^3.

according to our calculations (Fig. 7), the classical deformation mode—generation and glide of lattice dislocations—is more favorable than the nanodisturbance deformation mode in Au nanowires with steps at given values of the nanowire size and the external stress.

Commonly, the probability of the existence of steps at nanowire free surfaces increases with increasing nanowire sizes. As a corollary, with the results of our theoretical examination, it is logical to expect that the nanodisturbance deformation mode (classical dislocation slip, respectively) tends to dominate with decreasing (increasing, respectively) nanowire sizes. In particular, the nanodisturbance deformation mode can effectively occur in nanowires having ultrasmall sizes.

When mechanical load is absent, steps can be formed at nanowire free surfaces owing to thermally activated diffusion processes on such surfaces and in near-surface regions. In this context, an increase in temperature enhances both the formation of steps at the nanowire free surfaces and, if the mechanical load is applied to the nanowire, the classical dislocation slip.

Also, thermal fluctuations can directly assist plastic deformation occurring through either the classical dislocation slip or nanodisturbance deformation mode in nanowires. However, the role of temperature in direct enhancement of plastic flow in nanowires is significant, only if the external stress is very close to the critical stress for the athermal deformation. It is a narrow range of stresses. Our estimates (not presented here) show that, within this range of stresses, the thermally assisted events of plastic deformation hardly influence the competition between conditions of classical dislocation slip and the nanodisturbance deformation mode. Thus, the key role of temperature is in the enhancement of the formation of steps at nanowire free surfaces.

V. GEOMETRY, ENERGY, AND STRESS CHARACTERISTICS OF TWIN FORMATION OCCURRING THROUGH NANODISTURBANCES IN fcc NANOWIRES

In previous sections, we considered the generation of isolated nanodisturbances in a nanowire under tensile load. At the same time, there is another interesting situation where a nanodisturbance is formed at a crystallographic plane neighboring a preexisting stacking fault [Figs. 8(a), 8(b) and 8(c)] (which may result from evolution of a previously generated nanodisturbance). In this situation, the defect configuration consisting of the stable stacking fault and the nanodisturbance serves as a nucleus of a deformation twin in the nanowire. More precisely, when the nanodisturbance transforms into a stable stacking fault, a twin nucleus is generated, consisting of two stable stacking faults of nanoscopic size [Fig. 8(d)]. Similar defect configurations (called microtwins) have been theoretically considered in papers[27,36–38] focusing on the competition between lattice dislocation slip and twin formation in bulk materials. Following calculations,[27,36–38] the energy of a generalized stacking fault growing in a plane neighboring the preexisting stable stacking fault is different from that of a sole generalized stacking fault. Also, the stress concentration that is likely to exist at the surface step from which the initial stacking fault has been created may also help in the nucleation of the another nanodisturbance. Therefore, conditions for the formation of a nanoscale twin nucleus through the nanodisturbance deformation mode in a fcc nanowire (Fig. 8) are different from those of isolated nanodisturbances [Figs. 1(g)–1(i) and 1(l)–1(n)].

Let us calculate the energy change ΔW_t characterizing the generation of a twin nucleus through the nanodisturbance deformation mode (Fig. 8). In the framework of the proposed model (Fig. 8), the energy change ΔW_t in fact specifies the generation of a nanodisturbance in a crystallographic plane neighboring a preexisting stable stacking fault. The discussed situation (Fig. 8) is different from the previously considered situation with isolated nanodisturbances Sec. III
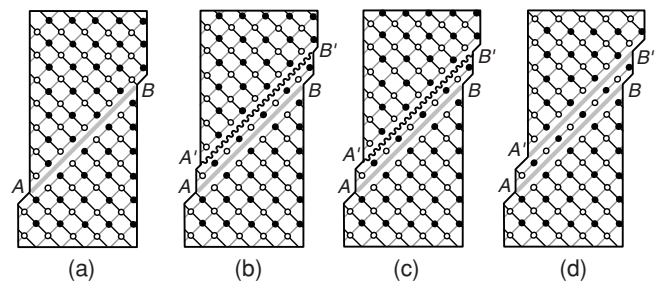

FIG. 8. Generation of twin nucleus by the nanodisturbance mode in a nanowire: Two-dimensional view in a crystallographic plane of a nanowire with a cubic elementary cell containing atoms of two types (full and open circles). (a) The nanowire is in its initial state with stable stacking fault AB (which may result from the evolution of a previously generated nanodisturbance). (b) and (c) A nanodisturbance $A'B'$ is generated and evolves in a crystallographic plane neighboring the preexisting stacking fault. (d) The nanodisturbance transforms into a stable stacking fault (neighboring the preexisting stacking fault). As a result, a nanoscale twin nucleus is generated that consists of two stable stacking faults AB and $A'B'$.

in the following two aspects. First, the initial configuration contains a stable stacking fault [Fig. 8(a)] having an energy $\gamma_{\text{isf}}\sqrt{3}d^2$ (with $\sqrt{3}d^2$ being the rhombic slip plane area). Second, a generalized stacking fault with energy W_{tf} is generated and evolves in a crystallographic plane neighboring a preexisting stable stacking fault [Figs. 8(b) and 8(c)], instead of an isolated generalized stacking fault (with energy W_{gsf}) (Fig. 1). In these circumstances, the energy change ΔW_t can be written as follows:

$$\Delta W_t = W_d + W_s + W_{tf} - \gamma_{\text{isf}}S - A, \qquad (11)$$

where W_d, W_s, S, and A are given by formulas (4)–(8). The energy W_{tf} of the generalized stacking fault having a stable stacking fault in a neighboring plane (Fig. 8) is as follows:

$$W_{\text{tf}} = \gamma_{\text{tf}}(s)S, \qquad (12)$$

where $\gamma_{\text{tf}}(s)$ is the specific energy of the generalized stacking fault in question. With results from Ref. 36, the function γ_{tf} of s can be approximated by the following formula:

$$\gamma_{\text{tf}}(s/b)$$
$$= \begin{cases} \gamma_{\text{isf}} + \frac{\gamma_{\text{ut}} - \gamma_{\text{isf}}}{2}\left(1 - \cos\frac{2\pi s}{b}\right), & 0 \leqslant s/b < 1/2, \\ \frac{\gamma_{\text{ut}} + 2\gamma_{\text{tsf}}}{2} - \frac{\gamma_{\text{ut}} - 2\gamma_{\text{tsf}}}{2}\cos\frac{2\pi s}{b}, & 1/2 \leqslant s/b < 1. \end{cases} \qquad (13)$$

Here γ_{ut} is the maximum value of $\gamma_{\text{tf}}(s)$, corresponding to the unstable configuration of the generalized stacking fault

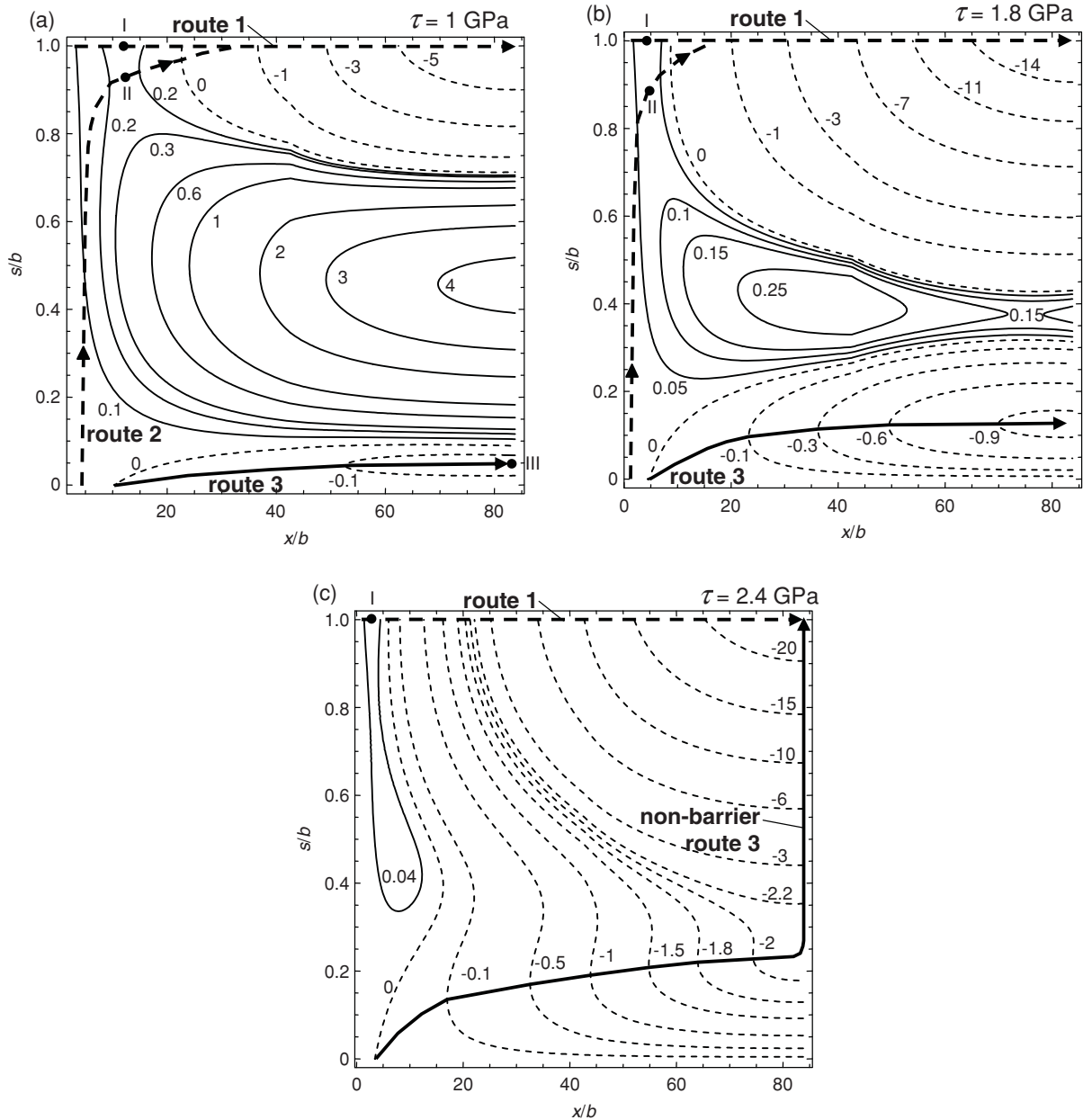

FIG. 9. Maps of the energy change $\Delta W_t(x,s)$ in the case of a Au nanowire (with size $d = 1$ nm) under the external shear stress (a) $\tau = 2.8$ GPa, (b) $\tau = 3.8$ GPa, and (c) $\tau = 4.5$ GPa. The values of ΔW_t are given in units of Db^3.
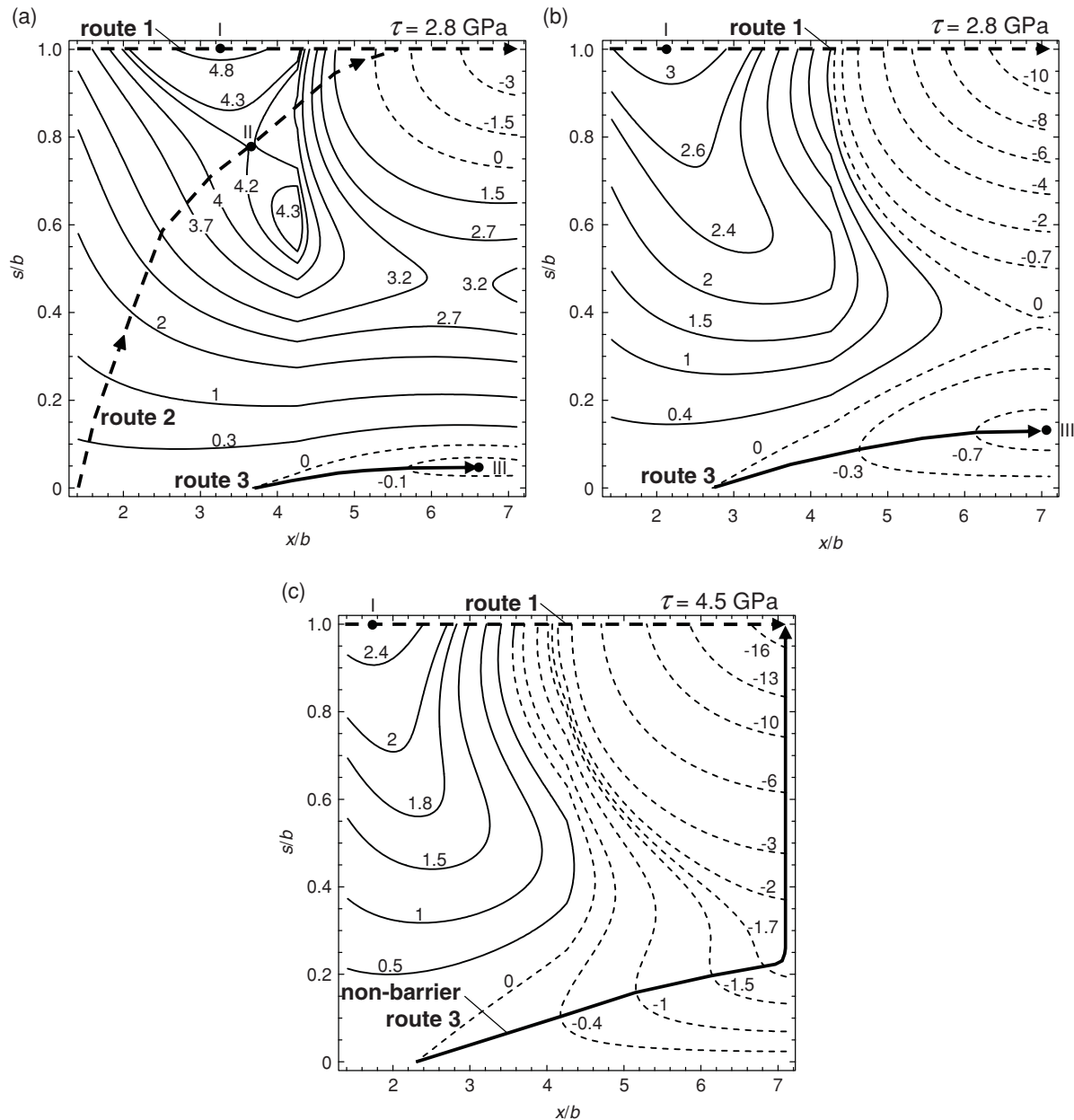
FIG. 10. Maps of the energy change $\Delta W_t(x,s)$ in the case of a Au nanowire (with size $d = 10$ nm) under the external shear stress (a) $\tau = 1$ GPa, (b) $\tau = 1.8$ GPa, and (c) $\tau = 2.4$ GPa. The values of ΔW_t are given in units of 10^2 Db^3.

(Fig. 8), and γ_{tsf} is the energy of the generalized stacking fault in its stable configuration (Fig. 8). In the case of Au, one has[36] $\gamma_{ut} = 0.148$ J/m^2 and $2\gamma_{tsf} = 0.031$ J/m^2.

We calculated the energy maps $\Delta W_t(x,s)$ for a Au nanowire with sizes $d = 1$ nm (Fig. 9) and $d = 10$ nm (Fig. 10) at different values of the external stress. The energy maps for twin nucleation (Figs. 9 and 10) are very similar to those for the formation of isolated nanodisturbances (Figs. 4 and 5) in deformed fcc nanowires. In this context, all the conclusions (formulated in Sec. III) concerning isolated nanodisturbances come into play in the case of twin nucleation as well. More precisely, there exist three possible routes of nanoscale twinning deformation (see routes 1–3 presented in Figs. 9 and 10). Route 1 corresponds to the conventional twinning micromechanism

through emission and movement of crystallographic partial dislocations (Fig. 11). Route 2 corresponds to the twinning micromechanism associated with the nanodisturbance deformation mode (Fig. 8). Routes 1 and 2 are specified by nonzero energy barriers [Figs. 9(a) and 10(a)]. At the same time, nonbarrier route 3 corresponds to the twinning micromechanism associated with the nanodisturbance deformation mode (Fig. 8). Evolution of the system through nonbarrier route 3 at intermediate stresses [Figs. 9(b) and 10(b)] stops at the state [$x = (d - b)\sqrt{2}$, $s \approx 0.1b$], but does not reach the final state [$x = (d - b)\sqrt{2}$, $s = b$] in which a nanoscale two-layer twin [Fig. 8(d)] is generated. Evolution of the system through nonbarrier route 3 reaches the final state [$x = (d - b)\sqrt{2}$, $s = b$] only at a high level of applied stresses [Figs. 9(c) and
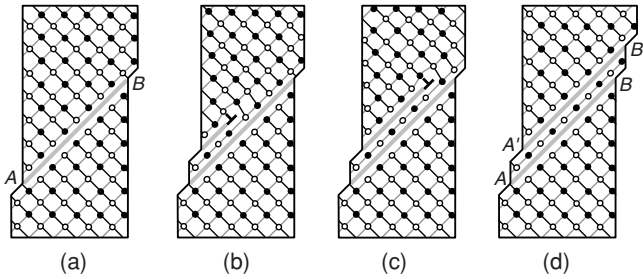
FIG. 11. Generation of a twin nucleus by the dislocation mechanism in a nanowire: Two-dimensional view in a crystallographic plane of a nanowire with a cubic elementary cell containing atoms of two types (full and open circles). (a) The nanowire is in its initial state with stable stacking fault AB. (b) and (c) A partial dislocation glides on a crystallographic plane neighboring the preexisting stacking fault. (d) The dislocation glide is complete, in which case a nanoscale twin nucleus (consisting of two stable stacking faults AB and $A'B'$) is generated.

10(c)]. Thus, according to our calculations (Figs. 9 and 10), the nonbarrier formation of nanoscale deformation twins in nanowires can occur through the nanodisturbance deformation mode (Fig. 8) when the applied stresses are high.

In addition, from Figs. 4, 5, 9, and 10, it follows that the nanoscale twin nucleation (Fig. 8) is more energetically
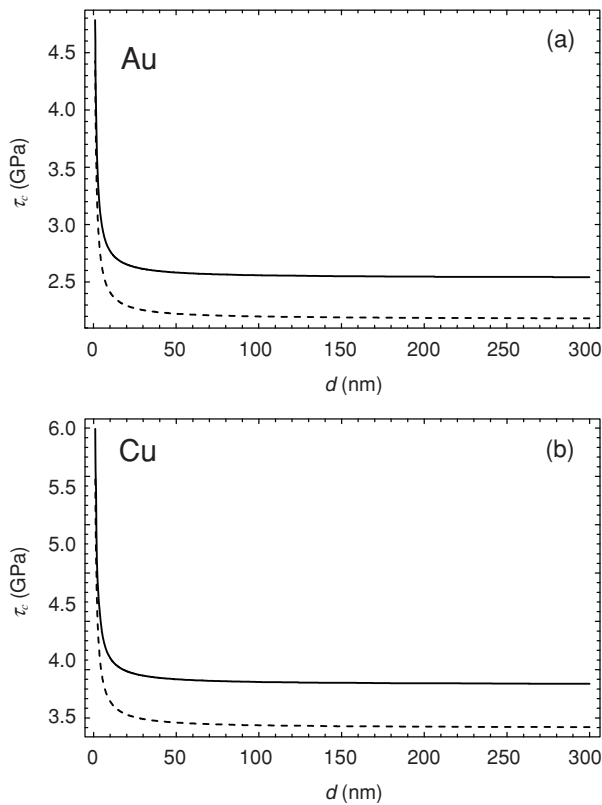

FIG. 12. Dependences of the critical stress τ_c (the smallest stress at which the nanodisturbance deformation mode occurs in the nonbarrier way) on the nanowire size d in (a) Au and (b) Cu nanowires. Solid curves correspond to the formation of an isolated nanodisturbance. Dashed curves correspond to the formation of a nanoscale twin nucleus.

favorable than the formation of isolated nanodisturbances (Fig. 1) and stable stacking faults (Fig. 2). In order to illustrate this fact, we calculated the dependences of the critical stress τ_c (the smallest stress at which the deformation occurs in the nonbarrier way) on the nanowire size d, for Au and Cu, in both the cases of the nanoscale twin nucleation and formation of isolated stacking faults through the nanodisturbance deformation mode (Fig. 12). For Cu, we used the following values of parameters: $G = 48$ GPa, $\nu = 0.34$, $\gamma_s = 1.725$ J/m^2,[34] $\gamma_{us} = 0.18$ J/m^2, $\gamma_{isf} = 0.041$ J/m^2, $\gamma_{ut} = 0.2$ J/m^2, and $2\gamma_{tsf} = 0.04$ J/m^2.[36] The calculated dependences show that the values of the critical stress τ_c characterizing the twin nucleation are lower (by ∼15%) than those characterizing the formation of isolated stacking faults in Au [Fig. 12(a)] and Cu [Fig. 12(b)] nanowires. The same result is expected to be valid for any fcc metal whose energy characteristics γ_{isf}, γ_{us}, and γ_{ut} satisfy inequality $\gamma_{ut} - \gamma_{isf} < \gamma_{us}$.

The dependences in Fig. 12 are indicative of a size effect ("smaller is stronger") in the considered range of d from 1 to 300 nm. Also, note that the critical stress in Au and Cu nanowires with $d = 10$ nm has very high values. For Au, we find $\tau_c \approx 0.1\,G$ in the case of isolated nanodisturbances, and $\tau_c \approx 0.09\,G$ in the case of nanoscale deformation twins [Fig. 12(a)]. For Cu, we have $\tau_c \approx 0.09\,G$ in the case of isolated nanodisturbances, and $\tau_c \approx 0.08\,G$ in the case of nanoscale deformation twins [Fig. 12(b)]. In the latter case (Cu), the values of the shear stress τ_c fall in the range (from 0.02 to 0.09 G) measured in the room-temperature experiment[22] with the tensile load of Cu nanowires having linear sizes of their cross sections in the range from 75 to 280 nm.

VI. CONCLUDING REMARKS

Thus, a specific physical mechanism of plastic flow—the nanodisturbance deformation mode associated with the formation and evolution of near-surface nanodisturbances [Figs. 1(g)–1(i) and 1(l)–1(n)]—can occur in strained nanowires with a fcc crystal structure owing to the nanoscale and free-surface effects. Also, nucleation and growth of nanoscale deformation twins can be realized through successive generation and evolution of nanodisturbances at neighboring crystallographic planes (Fig. 8). With the results of our calculations of the energy characteristics (Figs. 4 and 5), the nanodisturbance deformation dominates over conventional dislocation generation and glide in ideal Au nanowires at high stresses and zero temperature. At the same time, in Au nanowires with steps at their free surfaces (Fig. 6), the classical deformation mode—generation and glide of lattice dislocations—is more energetically favorable than the nanodisturbance deformation mode.

Also, we theoretically examined the role of the nanodisturbance deformation mode in the generation of nanoscale twins in mechanically loaded fcc nanowires. It has been shown that, in nanowires under high applied stresses, the nonbarrier formation of nanoscale deformation twins can effectively occur through the nanodisturbance deformation mode (Fig. 8). Also, from Figs. 4, 5, 9, and 10, it follows that the nanoscale twin nucleation (Fig. 8) is more favorable than the formation of isolated nanodisturbances (Fig. 1) and stable stacking faults (Fig. 2). Values of the critical stress τ_c—the smallest

stress at which the nanodisturbance deformation occurs in a nonbarrier way—for nanoscale twinning deformation are lower (by $\sim$15%) than those for the formation of isolated nanodisturbances in Au and Cu nanowires (Fig. 12). The critical stress τ_c is sensitive to nanowire size d. In the considered range of d from 1 to 300 nm, the dependences $\tau_c(d)$ show a clear size effect ("smaller is stronger") (Fig. 12). When nanowires are specified by an ultrasmall width, the values of the critical stress τ_c are very high. For instance, in the case of the formation of isolated nanodisturbances in nanowires with $d = 10$ nm, the critical stress has values of $\tau_c \approx 0.1\,G$ for Au [Fig. 12(a)] and $\tau_c \approx 0.08\,G$ for Cu [Fig. 12(b)].

The suggested theoretical representations on the nanodisturbance deformation mode in nanowires [Figs. 1(f)–1(o) and 2] are indirectly supported by the following experiments and computer simulations: (i) the experiment[25] concerning plastic deformation (thinning) of Au nanowires, (ii) the experiment[28] with plastic deformation of Gum metals, and (iii) results[32] of molecular-dynamics simulations of plastic flow in nanometer-sized single crystals having an approximately spherical shape (for details, see the discussion in Sec. III).

The suggested representations on the nanodisturbance deformation mode are worth being taken into account in future experimental and theoretical examinations of the deformation behavior of nanowires. Of special importance would be an experimental *in situ* observation of the nanodisturbance formation during plastic deformation of nanowires with ultrasmall sizes and various compositions. This will allow one to experimentally identify the conditions at which the nanodisturbance deformation mode is dominant. Finally, the nanodisturbance deformation mode is of large fundamental interest as a physical deformation mechanism that can contribute to plastic flow in both composite solids containing nanowires
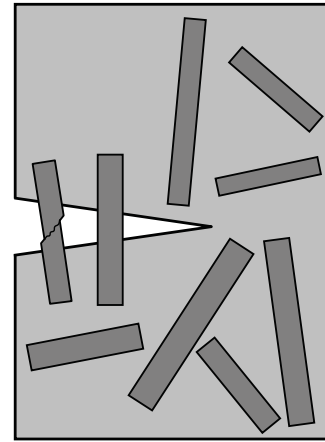

FIG. 13. Crack growth in a composite solid with nanowires (shown schematically). Metallic nanowires are under plastic deformation in the wake of brittle crack tip. They hamper crack growth.

(Fig. 13) and nanowires with preexisting plane defects such as grain, twin, and interphase boundaries (that recently attracted much interest[39–42]).

*Corresponding author: ovidko@nano.ipme.ru

[1] J. Schiotz, T. Vegge, F. D. Di Tolla, and K. W. Jacobsen, Phys. Rev. B **60**, 11971 (1999).

[2] H. Van Swygenhoven, M. Spaczer, A. Caro, and D. Farkas, Phys. Rev. B **60**, 22 (1999).

[3] I. A. Ovid'ko, Science **295**, 2386 (2002).

[4] I. A. Ovid'ko, Phys. Rev. Lett. **88**, 046103 (2002).

[5] D. Farkas, M. Willemann, and B. Hyde, Phys. Rev. Lett. **94**, 165502 (2005).

[6] S. V. Bobylev, N. F. Morozov, and I. A. Ovid'ko, Phys. Rev. Lett. **105**, 055504 (2010).

[7] J. C. M. Li, Phys. Rev. Lett. **96**, 215506 (2006).

[8] K. E. Aifantis, A. L. Kolesnikova, and A. E. Romanov, Philos. Mag. **87**, 4731 (2007).

[9] X. L. Wu and Y. T. Zhu, Phys. Rev. Lett. **101**, 025503 (2008).

[10] I. Zizak, N. Darowski, S. Klaumunzer, G. Schumacher, J. W. Gerlach, and W. Assmann, Phys. Rev. Lett. **101**, 065503 (2008).

[11] A. Cao and Y. Wei, Phys. Rev. B **74**, 214108 (2006).

[12] M. D. Uchic, D. M. Dimiduk, J. N. Florando, and W. D. Nix, Science **305**, 986 (2004).

[13] H. S. Park, K. Gall, and J. A. Zimmerman, Phys. Rev. Lett. **95**, 255504 (2005).

[14] J. R. Greer and W. D. Nix, Phys. Rev. B **73**, 245410 (2006).

[15] J. R. Greer, Rev. Adv. Mater. Sci. **13**, 59 (2006).

[16] Z. W. Shan, R. K. Mishra, S. A. Syed Asif, O. L. Waren, and A. M. Minor, Nature Mater. **7**, 115 (2007).

[17] H. Bei, S. Shim, E. P. George, M. K. Miller, E. G. Herbert, and G. M. Pharr, Scr. Mater. **57**, 397 (2007).

[18] E. Rabkin and D. J. Srolovitz, Nano Lett. **7**, 101 (2007).

[19] T. Zhu, J. Li, A. Samanta, A. Leach, and K. Gall, Phys. Rev. Lett. **100**, 025502 (2008).

[20] S. Brinckmann, Ju-Young Kim, and J. R. Greer, Phys. Rev. Lett. **100**, 155502 (2008).

[21] H. Tang, K. W. Schwarz, and H. D. Espinosa, Phys. Rev. Lett. **100**, 185503 (2008).

[22] G. Richter, K. Hillerich, D. S. Gianola, R. Mönig, O. Kraft, and C. A. Volkert, Nano Lett. **9**, 3048 (2009).

[23] A. T. Jennings, M. J. Burek, and J. R. Greer, Phys. Rev. Lett. **104**, 135503 (2010).

[24] S. V. Bobylev and I. A. Ovid'ko, Phys. Rev. Lett. **103**, 135501 (2009).

[25] Y. Kurui, Y. Oshima, M. Okamoto, and K. Takayanagi, Phys. Rev. B **79**, 165414 (2009).

[26] G. Lu, N. Kioussis, V. V. Bulatov, and E. Kaxiras, Phys. Rev. B **62**, 3099 (2000).

[27] N. Bernstein and E. B. Tadmor, Phys. Rev. B **69**, 094116 (2004).

[28] J. P. Cui, Y. L. Hao, S. J. Li, M. L. Sui, D. X. Li, and R. Yang, Phys. Rev. Lett. **102**, 045503 (2009).

[29] M. Yu. Gutkin, T. Ishizaki, S. Kuramoto, and I. A. Ovid'ko, Acta Mater. **54**, 2489 (2006).

[30] M. Yu. Gutkin and I. A. Ovid'ko, Appl. Phys. Lett. **88**, 211901 (2006).

[31] M. Yu. Gutkin and I. A. Ovid'ko, Acta Mater. **56**, 1642 (2008).

[32] L. Sun, A. V. Krasheninnikov, T. Ahlgren, K. Nordlund, and F. Banhart, Phys. Rev. Lett. **101**, 156101 (2008).

[33] J. P. Hirth and J. Lothe, *Theory of Dislocations* (Wiley, New York, 1982).

[34] I. A. Ovid'ko and A. G. Sheinerman, Phys. Rev. B **66**, 245309 (2002).

[35] F. Glas, Phys. Rev. B **74**, 121302(R) (2006).

[36] S. Kibey, J. B. Liu, D. D. Johnson, and H. Sehitoglu, Acta Mater. **55**, 6843 (2007).

[37] E. B. Tadmor and S. Hai, J. Mech. Phys. Solids **51**, 765 (2003).

[38] S. Ogata, J. Li, and S. Yip, Phys. Rev. B **71**, 224102 (2005).

[39] K. Zhou, A. A. Nazarov, and M. S. Wu, Phys. Rev. Lett. **98**, 035501 (2007).

[40] M. S. Wu, K. Zhou, and A. A. Nazarov, Phys. Rev. B **76**, 134105 (2007).

[41] A. Cao and Y. G. Wei, Phys. Rev. B **74**, 214108 (2006).

[42] N. Abdolrahim, I. N. Mastorakos, and H. M. Zbib, Phys. Rev. B **81**, 054117 (2010).